Alnak, D. E., *et al.*: Analysis of Heat and Mass Transfer of the Different Moist ...
THERMAL SCIENCE: Year 2018, Vol. 22, No. 6B, pp. 2943-2953

2943

ANALYSIS OF HEAT AND MASS TRANSFER OF THE DIFFERENT MOIST OBJECT GEOMETRIES WITH AIR SLOT JET IMPINGING FOR FORCED CONVECTION DRYING

by

Dogan Engin ALNAK[a] and Koray KARABULUT[b]*

[a] Automotive Engineering Department, Technology Faculty,
Sivas Cumhuriyet University, Sivas, Turkey
[b] Electric and Energy Department, Sivas Vocational High School,
Sivas Cumhuriyet University, Sivas, Turkey

In the present work, the effect of the different geometric moist objects with straight and reverse semi-circular on the heat and mass transfer enhancement of the jet drying was conducted with a numerical analysis. The drying jet was a laminar 2-D jet stationed at a constant jet distance from the moist object. The diameter of the object, jet distance from the moist object and initial jet height were fixed in all cases. Temperature and mass distributions were obtained inside the object for different jet velocities. A finite volume method was used to solve the governing equations for momentum and energy by using ANSYS Fluent 17.0 software program. Calculations were performed for four different Reynolds numbers, namely, Re = 100, 200, 300, and 400. It was found good agreement with the experimental data available in the literature. The results showed that the geometry of straight semi-circular moist object had better performance of heat and mass transfer than that of the reverse moist object geometry. In addition, increasing Reynolds number showed a positive effect on heat and mass transfer. Locally, jet drying was found to be most effective near the stagnation point on the leading side of the objects.
Key words: *drying, fluid-flow, jet impingement, mass transfer*

Introduction

Processes that employ jet impingement are widely used to increase heat and mass transfer in different engineering and industrial applications, such as food processing, fabrication of textiles and paper, and in air plane engines, to name a few. The geometry of impinged objects is mostly streamlined. Experimental and numerical methods were used to evaluate these kinds of problems, as summarized by Martin [1]. A numerical solution was obtained for unsteady 2-D fluid-flow and heat transfer in a confined impinging slot jet using the finite volume method by Lee *et al*. [2]. They found that the unsteadiness greatly affected the flow and temperature fields and, as a result, the pressure coefficient, skin friction coefficient, and Nusselt number in the unsteady region showed different characteristics from those in the steady region.

Tawfek [3] experimentally studied the effect of jet inclination on the local heat transfer under an obliquely impinging round air jet striking an isothermal circular cylinder. He measured the circumferential heat transfer distribution as well as axial Nusselt number and found that the shape of local heat transfer profiles was significantly affected by the jet inclination. Heat transfer

---

2944

Alnak, D. E., *et al.*: Analysis of Heat and Mass Transfer of the Different Moist ...
THERMAL SCIENCE: Year 2018, Vol. 22, No. 6B, pp. 2943-2953

from a slot air jet impinging on a cylinder at different Reynolds numbers and different cylinder curvatures was studied by Olsson *et al.* [4]. Rahman *et al.* [5] studied the heat transfer characteristics of a free jet discharging from a slot nozzle and impinging vertically on a curved plate of finite thickness using Galerkin's finite element method. They found that increasing the slot nozzle width decreased the local heat transfer coefficient but increased the local Nusselt number. Gori and Bossi [6], and Gori *et al.* [7] performed a series of experiments on jet impingement on a heated cylindrical object and obtained optimal parameters by measuring only the heat transfer. Teamah and Khairat [8] investigated experimentally the effect of interaction of the impinging circular double jets stream on the heat transfer coefficient by varying the interval between two jets, and also by changing the strength of one or both jets. They obtained that increment in the jet-to-jet spacing increases the average Nusselt number at the same Reynolds number. In another work, Hosain *et al.* [9] conducted numerical investigation of heat transfer by turbulent water jets impinging on a hot flat steel plate at temperatures below the boiling point in order to understand convection heat transfer phenomena of runout table cooling. They found that the thermal performance of a two-jet system was no better than a single jet because the jets were too far from each other to generate any additional thermal interaction. Slot jet impingement of air involving heat transfer from circular cylinders with different diameters was studied by McDaniel and Webb [10]. Eren *et al.* [11] correlated the stagnation point and local and average Nusselt numbers as functions of jet Reynolds number and dimensionless circumferential distance for a slot jet impinging on slightly curved convex and concave surfaces. Frost *et al.* [12] carried out experiments to measure the heat transfer from a constant heat flux flat plate to a axisymmetric jet with turbulent ($Re_d =$ 20.000) for distances ranging from 1d to 8d between nozzle and plate. They found to be maximum heat transfer at the stagnation point as the nozzle distance from the plate was around 6d. Chan *et al.* [13] carried out an experiment to obtain the effects of different parameters on the local heat transfer for an air slot jet impinging on a semicircular convex surface. They used a liquid crystal thermographic system to measure temperatures at different points. In another study, they studied the mean flow and turbulence of an air slot jet impinging on two different semicircular convex surfaces using a hot-wire X-probe anemometer [14]. Robinson and Schnitzler [15] studied for both free-surface and confined submerged jet arrays, heat transfer and pressure drop characteristics of liquid jet arrays impinging on a heated surface. It was found that submerged jet configuration displayed higher heat transfer coefficient at lower jet-to-jet spacing when compared to free-jet flows by requiring the lowest pumping power.

Another aspect of the current work deals with convective drying, which has been investigated by many researchers. Tarek and Ray [16] reviewed studies on drying simulation using CFD. They conducted a comprehensive review of both industrial- and lab-scale studies. They also investigated the sludge drying problem with numerical techniques [17]. The 2-D analysis of heat and mass transfer during drying of a rectangular moist object was performed by Kaya *et al.* [18] using an implicit finite difference method, with convective boundary conditions at all surfaces of the moist object. They found that the convective heat transfer coefficient varied from 4.33 to 96.16 $W/m^2 K$, and the convective mass transfer coefficient ranged from $9.28 \cdot 10^{-7}$ to $1.94 \cdot 10^{-5}$ m/s at various aspect ratios. Alnak *et al.* [19] carried out a investigation about jet drying of a moist cylinder with numerical analysis. They obtained temperature and mass distributions inside the object for different jet velocities (Re = 100, 200, and 300) and three different distances (D/H = 0.22, 0.25, and 0.33) from the moist cylinder, and also found that heat and mass transfer enhanced with reducing the distance between the jet and cylinder. Kaya *et al.* [20] conducted both experimental and numerical studies on heat and mass transfer during the drying of kiwi fruit. The time-dependent temperature and moisture distributions for different

Alnak, D. E., *et al.*: Analysis of Heat and Mass Transfer of the Different Moist ...
THERMAL SCIENCE: Year 2018, Vol. 22, No. 6B, pp. 2943-2953

2945

cases were obtained using a code developed to investigate heat and mass transfer processes inside fruit. The 2-D numerical heat and moisture transfer during the drying of a cylindrical object using an explicit finite difference was performed by Hussain and Dincer [21]. Oztop and Akpinar [22] numerically analyzed the heat and mass transfer of drying of different fruits by comparing experimental data from a cyclone dryer. Kadem *et al*. [23] investigated characteristics of wood microwave drying by solving 3-D Navier-Stokes equations for the fluid field and Luikov model with Lambert's law in 3-D fort he porous solid (wood) during drying process. The results showed that the variations of irradiation time, microwave power level, and sample thickness played an important role in overall drying kinetics.

Similarly, in another study, Younsi *et al*. [24] carried out numerical solutions for wood of 3-D equations for coupled heat and mass conservation equations by using a commercial package Femlab. They determined that the simulation of the proposed conjugate problem allowed the assessment of the effect of the heat and mass transfer within wood.

The main aim of the present study was to investigate the effect of the different semi-circular moist objects with straight and reverse geometry on the fluid-flow, heat and mass transfer due to a slot jet impingement. This study was one of the important attempts to research both heat and mass transfer of free slot-jet impingement in different geometric moist objects. The effect of the Reynolds number on the local Nusselt number variation was examined both for the semi-circular objects and also temperature and concentration profiles along the middle *x*-axis of the moist objects were studied. Calculations were carried out by using the ANSYS FLUENT 17.0 software program [25]. The numerical results published previously by Varol *et al*. [26] were shown to be in good agreement with the experimental data carried out by Gori *et al*. [27] to validate the model. The results were presented as streamlines, isotherms, temperature and concentration profiles variations along the middle *x*-axis of the moist objects and the Nusselt number distribution for different moist objects and Reynolds numbers.

Physical model

The physical model considered is shown in fig. 1(A). The figure shows a schematic view of the system with boundary conditions. A slot jet impinges onto moist semi-circular objects. The objects have a constant diameter and a *x*-location. The air leaves the jet nozzle with
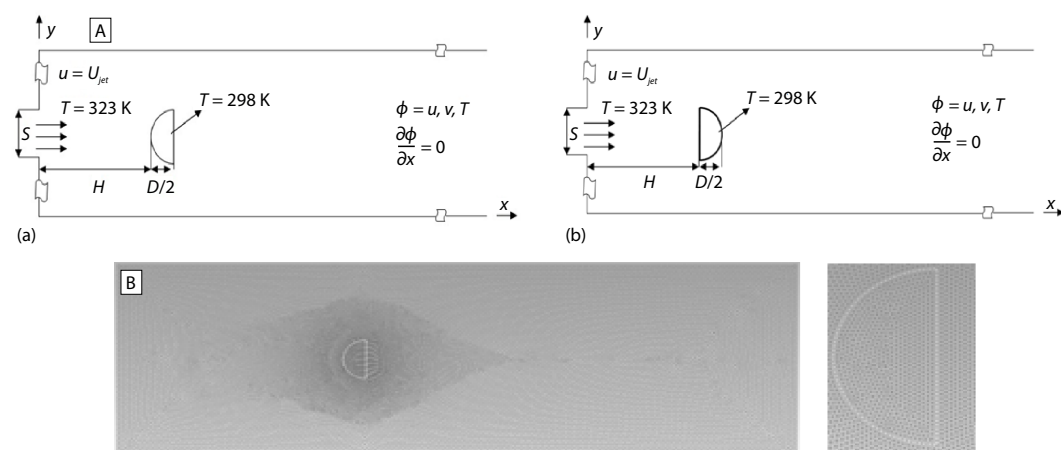

Figure 1. Shematic views of the considered models: A – physical model with boundary conditions, (a) straight semi-circular object, (b) reverse semi-circular object, B – grid distribution

2946

Alnak, D. E., *et al.*: Analysis of Heat and Mass Transfer of the Different Moist ...
THERMAL SCIENCE: Year 2018, Vol. 22, No. 6B, pp. 2943-2953

constant temperature and velocity. The cylinder diameter, D, and nozzle, S, are both equal to 0.4 cm. Other boundaries are placed far from the object to eliminate their effect on the solution.

Numerical method

The numerical study has been conducted to study the 2-D, steady, laminar incompressible fluid-flow, conjugate heat transfer of forced convection and conduction in a object surface and forced convection drying in a moist semi-circular object. The finite volume method (FLUENT program) was used to solve the conjugate heat and mass transfer analysis.

The finite volume method is based on the principle of dividing the geometry which will be solved in portions to find a solution for each of these sections and then by uniting these solutions to find a general solution to the problem. This method uses a technique which is based on the control volume for transforming heat flow equations into algebraic equations which can be solved numerically. In other words, this technique is based on the principle of taking the heat flow equations integration in each control volume. This integration result provides equations which characterize each control volume which occurs. For preparing the most appropriate grid model, a fine grid should be formed in regions where the change in variables such as velocity, pressure and temperature is bigger. A grid independence test was carried out by comparing the results of different grid meshes as shown in tab. 1. The test indicates that 57800 grids are adequate (<0.1% difference compared with 98712 grids). The grid distribution is shown in fig. 1(B) with 57800 elements. A structured grid is applied around the semi-circular objects. Convergence of the computations is stopped for the continuity and the momentum equations when residues are less than 10^{-6} and for the energy equation when residues are less than 10^{-6}.

Table 1. Grid independence test of the model

Grid name	Number of elements	Average Nusselt numbers			
		Re = 100	Re = 200	Re = 300	Re = 400
G1	25602	3.4515	5.7523	8.4825	10.9745
G2	42304	3.5412	5.8426	8.5765	10.9925
G3	57800	3.5501	5.8536	8.5877	11.0707
G4	98712	3.5542	5.8524	8.5865	11.0699
G5	153678	3.5541	5.5824	8.5865	11.0698

The governing equations for heat transfer and fluid-flow were simplified for steady 2-D laminar incompressible fluid-flow and constant fluid properties and also there was no heat generation or deformation inside the object. Body forces and viscous dissipation and heat radiation are ignored due to the weak temperature gradients in the flow. The resulting equations are expressed [25]:
– continuity equation

$$\frac{\partial u}{\partial x} + \frac{\partial v}{\partial y} = 0 \tag{1}$$

– momentum equation
– x-momentum equation

$$u\frac{\partial u}{\partial x} + v\frac{\partial u}{\partial y} = -\frac{1}{\rho}\frac{\partial p}{\partial x} + v\left(\frac{\partial^2 u}{\partial x^2} + \frac{\partial^2 u}{\partial y^2}\right) \tag{2}$$

– y-momentum equation

$$u\frac{\partial v}{\partial x}+v\frac{\partial v}{\partial y}=-\frac{1}{\rho}\frac{\partial p}{\partial y}+v\left(\frac{\partial^2 v}{\partial x^2}+\frac{\partial^2 v}{\partial y^2}\right) \tag{3}$$

– energy equation

$$u\frac{\partial T}{\partial x}+v\frac{\partial T}{\partial y}=\alpha\left(\frac{\partial^2 T}{\partial x^2}+\frac{\partial^2 T}{\partial y^2}\right) \tag{4}$$

where u and v are the velocity components, p – the pressure, v – the kinematic viscosity, ρ – the density of the fluid, T – the temperature of the fluid, and α – the thermal diffusivity. The boundary conditions can be stated as follows.

At the jet exit, $u = U_{jet}$, $T = 323$ K and at the channel outlet:

$$\frac{\partial \phi}{\partial x}=0 \tag{5}$$

At the top and bottom walls, $u = U_\infty$, $T = T_\infty$ and on the cylinder:

$$u = v = 0, \qquad T = 298 \text{ K} \tag{6}$$

The inlet Reynolds number is calculated:

$$\mathrm{Re}=\frac{uS}{v} \tag{7}$$

The local heat transfer coefficient is given:

$$-k\frac{\partial T}{\partial n}\bigg|_{w}=h\left(T_{w}-T_{\infty}\right) \tag{8}$$

and the local Nusselt number and Prandtl number are computed from:

$$\mathrm{Nu}=\frac{hD}{k}\quad\text{and}\quad\mathrm{Pr}=\frac{\mu c_{p}}{k} \tag{9}$$

The Prandtl number is taken as 0.71 for all cases. The 2-D equations of conduction heat transfer and mass transfer are written:

$$\frac{1}{\alpha}\frac{\partial T}{\partial t}=\frac{1}{r}\frac{\partial T}{\partial r}+\frac{\partial^2 T}{\partial r^2}+\frac{1}{r^2}\frac{\partial^2 T}{\partial \theta^2} \tag{10}$$

$$\frac{1}{D}\frac{\partial M}{\partial t}=\frac{1}{r}\frac{\partial M}{\partial r}+\frac{\partial^2 M}{\partial r^2}+\frac{1}{r^2}\frac{\partial^2 M}{\partial \theta^2} \tag{11}$$

These equations were solved by writing a user-defined function (UDF) code in FLUENT [25] using the following initial and boundary conditions:

$$T(r,\theta,t=0)=T_{i}\quad\text{and}\quad M(r,\theta,t=0)=M_{i} \tag{12}$$

$$\text{at}\quad r=0,\quad\frac{\partial T(0,\theta,t=t)}{\partial r}=0\quad\text{and}\quad\frac{\partial M(0,\theta,t=t)}{\partial r}=0 \tag{13}$$

$$\text{at}\quad r=R\quad -k\left[\frac{\partial T(R,\theta,t=t)}{\partial r}\right]=h(T_{w}-T_{\infty})\quad\text{and}\quad -D\left[\frac{\partial M(R,\theta,t=t)}{\partial r}\right]=h_{m}(M-M_{a}) \tag{14}$$

$$M(r,0,t)=M(r,\pi,t)\quad\text{and}\quad\frac{\partial M(r,0,t)}{\partial \theta}=\frac{\partial M(r,\pi,t)}{\partial \theta} \tag{15}$$

where D is the moisture diffusivity, h and h_m are the convective heat and mass transfer coefficients, respectively.

Validation

The numerical results of present study and obtained previously by Varol *et al.* [26] were compared with experimental data carried out experimentally by Gori *et al.* [27] to validate the model as shown in fig. 2. The local Nusselt number, fig. 2, was compared at different distances of the first and second cylinders (L/S). We can see some deviation from the published data, (Gori *et al.* [27], around $\theta = 45°$ and $150°$. However, excellent agreement was obtained for the cylinder at $L/S = 4$. This comparison showed that the grid distribution worked well for the considered problem, and also it was considered that this study would be suitable to evaluate the different moist semi object geometries for jet drying.
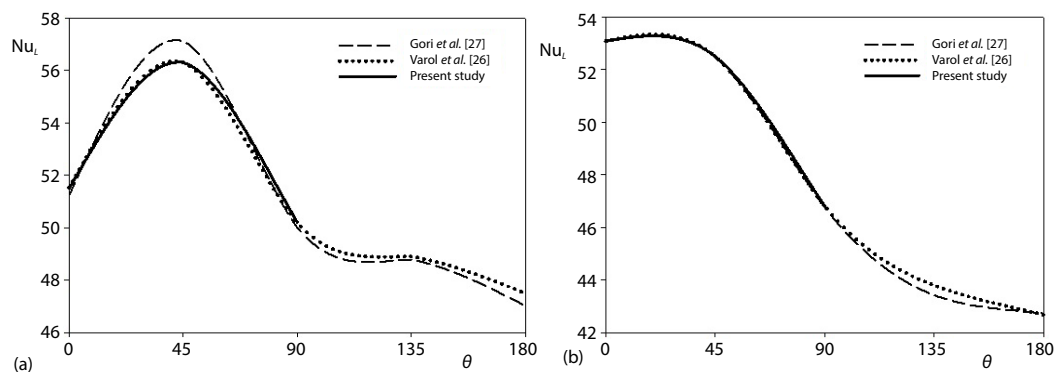

Figure 2. Comparison of local Nusselt numbers; (a) *L/S* = 2, and (b) *L/S* = 4

Results and discussion

The numerical results of a slot air jet impingement on two different semi-circular moist objects for fluid-flow and heat and mass transfer are presented and discussed. Results were attained for different Reynolds numbers and semi-circular moist objects. The Prandtl number was fixed as 0.71 for all cases.

Streamlines of straight and reverse semi-circular moist object for different inlet flow velocities are shown in figs. 3(a) and 3(b), respectively. A stagnation point occurred in front of the moist object with straight and reverse semi-circular where surface was normal to slot air jet impinging. As can be seen in fig. 3(a1), two eddies formed behind the straight semi-circular object and their dimensions became smaller with increased flow velocity. The flow oscillation occurred downstream of the semi-circular object and the frequency of oscillation increased with increasing Reynolds number. As seen in fig. 3(a2) at Re = 200, a large circulation cell occurred in the wake of the semi-circular object. When Reynolds number was increased to 300, the dimension of cell decreased and another circulation cell formed in the wake. In the case of Reynolds number of 400, fig. 3(a4), one of the cells disappeared behind the semi-circular. Figure 3(b) presents streamlines of reverse semi-circular moist object for different Reynolds numbers. As can be seen from fig. 3(b1), an eddy formed behind the reverse semi-circular object and its dimension became smaller with increased Reynolds number. Along with the oscillation frequency increased with increasing Reynolds number, the size of the eddy occurred in the wake of the reverse semi-circular became smaller as seen in fig. 3(b2-b4). It was interesting that the Reynolds

Alnak, D. E., *et al.*: Analysis of Heat and Mass Transfer of the Different Moist ...
THERMAL SCIENCE: Year 2018, Vol. 22, No. 6B, pp. 2943-2953

2949

number had an insignificant effect on the eddy formed behind the reverse semi-circular object as seen clearly from the figs. 3(b3) and 3(b4).
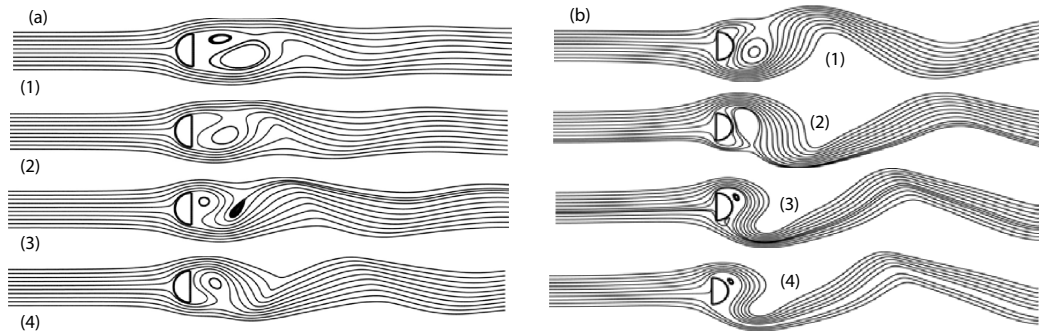

Figure 3. Streamlines of semi-circular moist objects (a) – straight, (b) – reverse for different Reynolds numbers; (1) Re = 100, (2) Re = 200, (3) Re = 300, and (4) Re = 400

Isotherms for straight and reverse semi-circular moist object with different values of Reynolds numbers are given in figs. 4(a) and 4(b). A general observation of isotherms clearly determines that the Reynolds number plays an important effect on the temperature distribution downstream of the straight and reverse semi-circular object as can be seen in figs. 4(a) and 4(b). Also it was obtained that the air temperature values of reverse semi-circular object were higher than that of straight semi-circular for all analyzed Reynolds numbers. This result indicated that the heat transfer to straight semi-circular moist object from impinging air slot jet was better than reverse object.
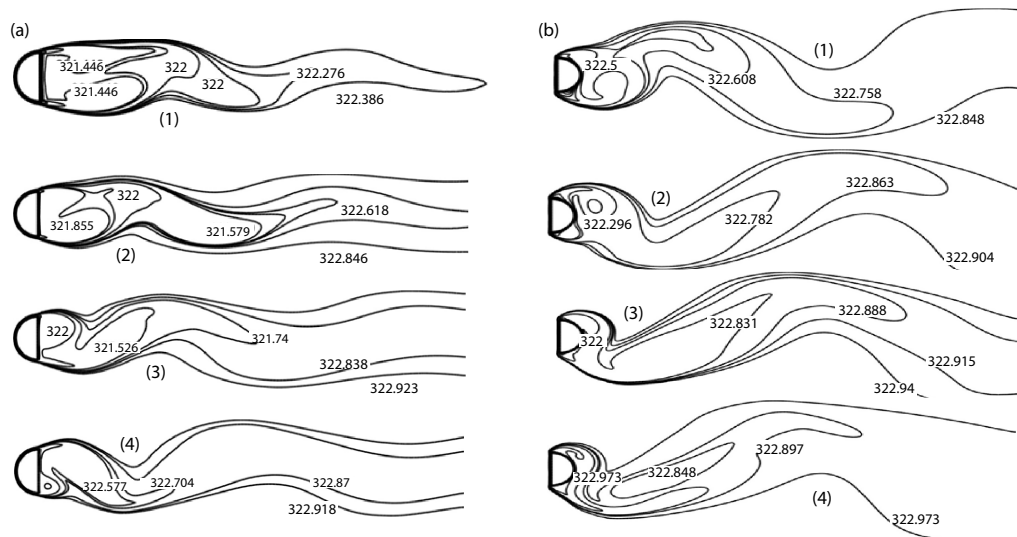

Figure 4. Isotherms for semi-circular moist objects (a) – straight (b) – reverse for different Reynolds numbers; (1) Re = 100, (2) Re = 200, (3) Re = 300, and (4) Re = 400

Figures 5(a) and 5(b) show the local Nusselt number variations along the perimeter of the straight and reverse semi-circular objects for different Reynolds numbers, respectively. As can be seen in fig. 5(a), the minimum value was obtained around $\theta = 45°$ for the Reynolds

numbers analyzed. However, the maximum values of local Nusselt number occurred between $\theta = 95°$ and $\theta = 135°$ but the values were strongly dependent on the Reynolds numbers. The minimum and maximum values of the Nusselt number were reached around at $\theta = 40°$ and $\theta = 90°$, respectively, for Re = 100 with reverse semi-circular object when there was a linear variation of the Nusselt number for the values of Re = 200, 300, and 400, fig. 5(b).
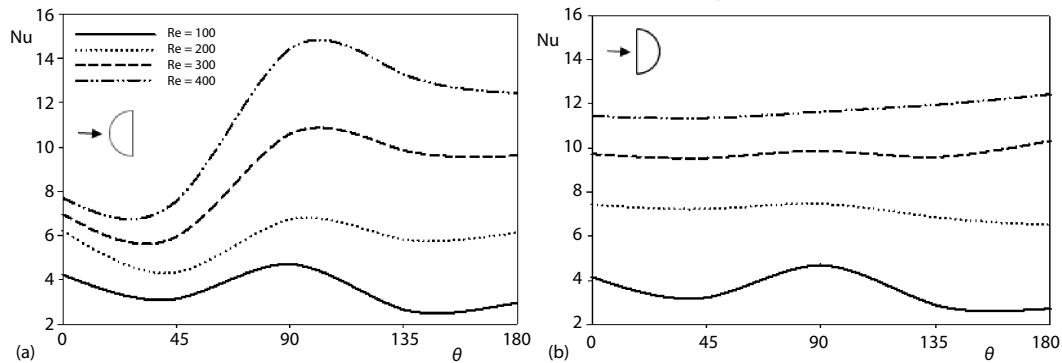

Figure 5. Local Nusselt number variations for different Reynolds number; (a) straight, (b) reverse semi-circular object

Figures 6(a) and 6(b) present the variations in temperature profiles along the middle *x*-axis of the straight and reverse semi-circular object at the different Reynolds numbers, respectively. The temperature values increased with increasing Reynolds number for both semi-circular objects. There were minimum values around $X = 0.38$ and $X = 0.52$ for the straight and reverse semi-circular objects, respectively. When the higher temperatures were found near the downstream region of the objects, the maximum temperatures were obtained for straight semi-circular comparing to reverse object.
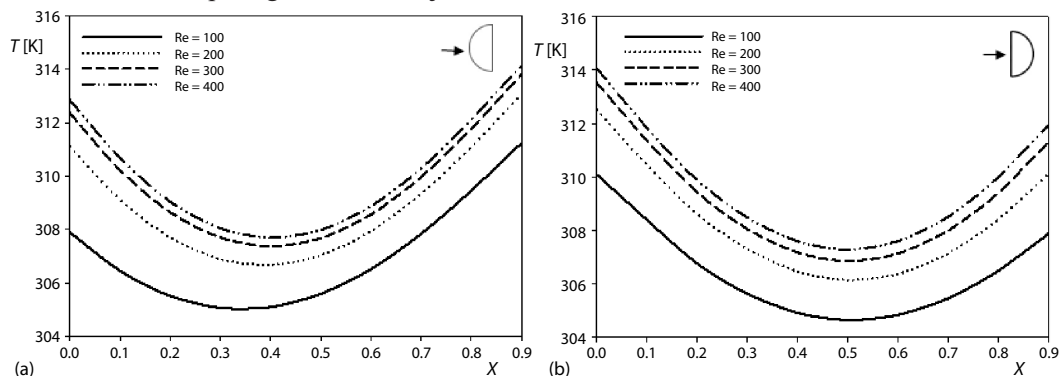

Figure 6. Temperature profiles variations along the middle x-axis of the semi-circular objects; (a) straight, (b) reverse

Figure 7 illustrates the concentration profiles variations through the middle *x*-axis of the straight and reverse semi-circular objects for the different Reynolds numbers, respectively. As can be seen in figs. 7(a) and 7(b), the concentration increased from the stagnation points to the inside the object and then it decreased to the downstream side of the straight and reverse semi-circular objects regarding to the temperature profiles, fig. 6. The highest concentration was seen in straight semi-circular object for all the analyzed Reynolds number values along the downstream region.
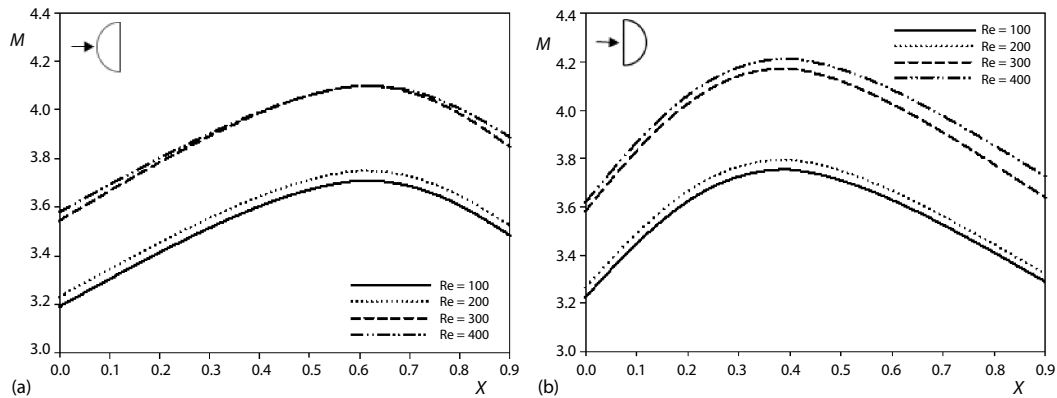
Alnak, D. E., *et al.*: Analysis of Heat and Mass Transfer of the Different Moist ...
THERMAL SCIENCE: Year 2018, Vol. 22, No. 6B, pp. 2943-2953

2951

**Figure 7. Concentration profiles variations along the middle *x*-axis of the moist objects;
(a) straight, (b) reverse**

Conclusions

The analysis of air jet drying of the new moist object geometries with straight and reverse semi-circular was investigated numerically using a finite volume method (ANSYS FLUENT 17.0). However, still no study could be found in the literature with regard to the effect of semi-circular moist object geometries with free slot-jet impingement researched in this study in drying with air jet. Therefore, it was necessary to investigate the heat and mass transfer performance characteristics of these types of geometries in order to obtain higher heat and mass transfer rates. Comparisons with previously published experimental data were performed and excellent agreement was found. The following conclusions were drawn from the present investigation.

- Both Reynolds number and geometry of the moist objects are important parameters on the heat and mass transfer. It was observed that the jet drying effectiveness improved with straight semi-circular moist object when comparing to reverse moist object.
- Circulation behind the semi-circular objects was directly related to Reynolds number. Multiple circulation cells were formed for higher Reynolds numbers. Heat transfer increased with increasing Reynolds number.
- The concentration value was higher at higher Reynolds number values and changed almost linearly downstream region along the *x*-axis inside the semi-circular objects.
- The numerical results were found to approximately agree with the experimental results and therefore it was considered that this study would be suitable for evaluating the jet drying performance of different moist semi object geometries.

Nomenclature

c_p – specific heat, [Jkg^{-1}K^{-1}]
D – semi-circular object radius, [m]
H – distance between slot exit and semi-circular moist object, [m]
h – heat transfer coefficient, [Wm^{-2}K^{-1}]
h_m – mass transfer coefficient, [ms^{-1}]
k – thermal conductivity, [Wm^{-1}K^{-1}]
L – distance between first and second cylinder, [m]
M – moisture distribution, [kgkg^{-1}]
Nu – Nusselt number, (=hD/k), [–]

Pr – Prandtl number, (= $\mu c_p/K$), [–]
Re – Reynolds number, (=$V_\infty d/v$), [–]
S – height of slot exit, [m]
T – temperature, [K]
t – time, [s]
u, v – velocities in x- and y-directions, [ms^{-1}]
x, y – co-ordinates, [–]

Greek symbols

μ – dynamic viscosity, [kgs^{-1}m^{-1}]

ν – kinematic viscosity, [m²s⁻¹]
ρ – density, [kgm⁻³]
ϕ – any dependent variables

Subscript

a – air
i – initial
w – wall
∞ – environment

References

[1] Martin, H., Heat and Mass Transfer between Impinging Gas Jets and Solid Surfaces, *Advances in Heat Transfer, 13* (1977), Dec., pp. 1-60

[2] Lee, H. G., *et al.*, A Numerical Investigation on the Fluid Flow and Heat Transfer in the Confined Imping-ing Slot Jet in the Low Reynolds Number Region for Different Channel Heights, *International Journal of Heat and Mass Transfer, 51* (2008), 15-16, pp. 4055-4068

[3] Tawfek, A. A., Heat Transfer Studies of the Oblique Impingement of Round Jets Upon a Curved Surface, *Heat and Mass Transfer, 38* (2002), 6, pp. 467-475

[4] Olsson, E. E. M., *et al.*, Flow and Heat Transfer from Multiple Slot Air Jets Impinging on Circular Cylin-ders, *Journal of Food Engineering, 67* (2005), 3, pp. 273-280

[5] Rahman, M. M., *et al.*, Free Liquid Jet Impingement from a Slot Nozzle to a Curved Plate, *Numerical Heat Transfer Part A, 57* (2010), 11, pp. 799-821

[6] Gori, F., Bossi, L., Optimal Slot Height in the Jet Cooling of a Circular Cylinder, *Applied Thermal Engi-neering, 23* (2003), 7, pp. 859-870

[7] Gori, F., *et al.* Cooling of Two Smooth Cylinders in Row by a Slot Jet of Air with Low Turbulence, *Ap-plied Thermal Engineering, 27* (2007), 14-15, pp. 2415-2425

[8] Teamah, M. A., Khairat, M. M., Heat Transfer Due to Imping Double Free Circular Jets, *Alexandria Engineering Journal, 54* (2015), 3, pp. 281-293

[9] Hosain, Md, L., *et al.*, Heat Transfer by Liquid Jets Impinging on a Hot Flat Surface, *Applied Energy, 164* (2016), Feb., pp. 934-943

[10] McDaniel, C. S., Webb, B. W., Slot Jet Impingement Heat Transfer from Circular Cylinders, *International Journal of Heat and Mass Transfer, 43* (2000), 11, pp. 1975-1985

[11] Eren, H., *et al.*, Non-Linear Flow and Heat Transfer Dynamics of Impinging Jets onto Slightly-Curved Surfaces, *Applied Thermal Engineering, 27* (2007), 14-15, pp. 2600-2608

[12] Frost, S. A., *et al.*, Heat Transfer from a Flat Plate to a Turbulent Axisymmetric Impinging Jet, *Proc. Inst. Mech. Eng., 211* (1997), 2, pp. 167-172

[13] Chan, T.L, *et al.* Heat Transfer Characteristics of a Slot Jet Impinging on a semi-Circular Convex Surface, *International Journal of Heat and Mass Transfer*, *45* (2002), 5, pp. 993-1006.

[14] Chan, T. L., *et al.*, Mean Flow and Turbulence Measurements of the Impingement Wall Jet on a Semi-Cir-cular Convex Surface, *Experiments in Fluids, 34* (2003), 1, pp. 140-149

[15] Robinson, A., Schnitzler, E., An Experimental Investigation of Free and Submerged Miniature Liquid Jet Array İmpingement Heat Transfer, *Experimental Thermal Fluid Science, 32* (2007), 1, pp. 1-13

[16] Tarek, J. J., Ray, M. B., Application of Computational Fluid Dynamics for Simulation of Drying Process-es: A Review, *Drying Technology, 28* (2010), 2, pp. 120-154

[17] Tarek, J. J., Ray, M. B., The Drying of Sludge in a Cyclone Dryer Using Computational Fluid Dynamics, *Drying Technology, 29* (2011), 12, pp. 1365-1377

[18] Kaya, A., *et al.* Numerical Modeling of Heat and Mass Transfer during Forced Convection Drying of Rect-angular Moist Objects, *International Journal of Heat and Mass Transfer, 49* (2006), 17-18, pp. 3094-3103

[19] Alnak, D. E., *et al.*, Simulation of Jet Drying of a Moist Cylinder at Low Reynolds Number, *Drying Tech-nology, 30* (2012), 6, pp. 631-640

[20] Kaya, A., *et al.* Experimental and Numerical Investigation of Heat and Mass Transfer during Drying of Hayward Kiwi Fruits (Actinidia Deliciosa Planch), *Journal of Food Engineering, 88* (2008), 3, pp. 323-330

[21] Hussain, M. M., Dincer, I., Two-Dimensional Heat and Moisture Transfer Analysis of a Cylindrical Moist Object Subjected to Drying: A Finite-Difference Approach, *International Journal of Heat and Mass Transfer, 46* (2003), 21, pp. 4033-4039

[22] Oztop, H. F., Akpinar, E. K., Numerical and Experimental Analysis of Moisture Transfer for Convective Dry-ing of Some Products, *International Communications in Heat and Mass Transfer, 35* (2008), 2, pp. 169-177

[23] Kadem, S., *et al.* Computational Analysis of Heat and Mass Transfer during Microwave Drying of Tim-ber, *Thermal Science*, *20* (2016), 5, pp. 1447-1455

[24] Younsi, R., *et al.*, Transient Analysis of Heat and Mass Transfer during Heat Treatment of Wood Including Pressure Equation, *Thermal Science*, *19* (2015), 2, pp. 693-702
[25] ***, FLUENT User's Guide Fluent Inc., 2003
[26] Varol, Y., *et al.*, Numerical Analysis of Heat Transfer due to Slot Jets Impingement onto Two Cylinders with Different Diameters, *International Communications in Heat and Mass Transfer*, *39* (2012), 5, pp. 726-735
[27] Gori, F., *et al.*, Cooling of Two Smooth Cylinders in Row by a Slot Jet of Air with Low Turbulence, *Applied Thermal Engineering, 27* (2007), 14-15, pp. 2415-2425